Van Hove Singularity and Weyl Points in Ferroelectrics-Based Acoustic Metamaterials

Zafer Ozer[1], Amirullah M. Mamedov[2,3], Ekmel Ozbay[2]

[1]Mersin University, Department of Electronics and Automation, 33160, Mersin, Turkey,

[2]Bilkent University, Nanotechnology Research Center, 06800, Ankara, Turkey,

[3]Baku State University, International Scientific Center, Baku, Azerbaijan,

*Corresponding e-mail: mamedov@bilkent.edu.tr

Abstract.

Weyl semimetals are materials in which the electrons have linear dispersions in all directions while being doubly degenerate at a single point, called a Weyl point, near the Fermi surface in 3D momentum space. Since the Weyl point or Weyl cone in Weyl semimetals represents a special dispersion of electrons moving in periodic potentials, the question naturally arises as to whether a similar dispersion or the Weyl point for classical waves propagating in artificial periodic structures exists. The study of Weyl points in electronic systems has inspired much recent research in classical systems such as photonic and acoustic lattices. We construct a single-phase three-dimensional structure, an analog of the honeycomb lattice, and predict the existence of Weyl points with opposite topological charges (±1) and the associated gapless topologically protected surface states. Following the developments of Weyl phononic crystals with Weyl points for acoustic waves, we report the theoretical investigation of Weyl points in ferroelectric-based 3D acoustic metamaterials. This study presented a fully continuous, load-bearing, elastic metamaterial capable of indirectionally propagating and topologically protected surface states. The design of the 3D unit cell, inspired by sandwich composites, consisted of a layered

prismatic lattice with different cross-sections in which the layers were spaced by solid cylindrical elements and by slanted circular beams connecting consecutive faces of the prismatic unit cell. The analysis of the lattice dynamics highlighted the existence of Weyl points following the breaking of the z-mirror symmetry and the P-symmetry of the lattice. To gain insight into the mechanism leading to the formation of these degenerate points, we evaluated the topological invariants using ab-initio calculations. This study may serve as a basis to develop composite-like structures having advanced elastic waveguiding capabilities for applications.

Keywords: Phononic Crystal, Weyl point, Acoustic Metamaterial, Finite Element Analysıs

1. Introduction

Weyl semimetal is a 3D (three-dimensional) topologically semimetal, which is a material whose band structure contains touching points that are topologically nontrivial and can host quasiparticle excitations that behave as Dirac or Weyl fermions [1-3]. These so-called Weyl points not only exist in electronic systems, but can also be found in artificial periodic structures with classical waves, such as acoustic waves in phononic crystals (PC). However, other than using complex 3D lattice structures, the realization of Weyl semimetals in low dimensions via the notion of synthetic dimension still remains elusive [4].

In the present investigation, we study an effective acoustic semimetal based on a class of structures that we call Weyl metamaterials [5]. In these systems, the chiral Weyl fermions are familiar from narrow band ferroelectrics. In present work, we also investigated various singularities

and behavioral features of the wave-matter interaction in the BZ based on Van Hove theory [6].

2. Method of calculation

In this research, we design a 3D elastic lattice made entirely of beams, which allows both translational and rotational degrees of freedom along their length directions. In this work, we design a bilayer PC with chiral interlayer interactions to realize ferroelectric-based quadratic Weyl semimetal hosting only a pair of quadratic WPs at the same high symmetry points of the Brillouin zone (*BZ*). C4 and time-reversal symmetries protect the existence of the quadratic WPs, which carry topological charges ±1, and possess quadratic dispersions along the k_x and k_y directions and a linear one along the k_z direction. Interestingly, we construct an interface formed by two different Weyl semimetals with opposite chirality of the interlayer interactions.

We design a PC with the unit cell on the basis of a bilayer structure, where each layer contains a crossed scatterer and is connected with the other layer by four chiral tubes drilled through a flat plate, as illustrated in Fig.1.

In our calculation, we use finite element analysis (FEA) to obtain a dispersion diagram for the unit cell and discuss its topological features in relation to Weyl physics. To conduct the numerical simulation, we use the commercial FEA software program COMSOL. We follow the method used in [6] to apply periodic boundary conditions and construct frequency-band diagrams. We used narrow band ferroelectric GeTe as the structural material with elastic modulus E = 496 GPa, density ρ= 61400 kg/m^3, and Poisson's ratio υ=0.61. We ignore any material dissipation. The out-of-plane beam produces an effective time-reversal symmetry at a fixed k_j (j=x, y, z). Therefore, the system can be treated as an elastic realization of the topological Haldane model (paradigmatic example of a Hamiltonian featuring topologically distinct phases of matter).

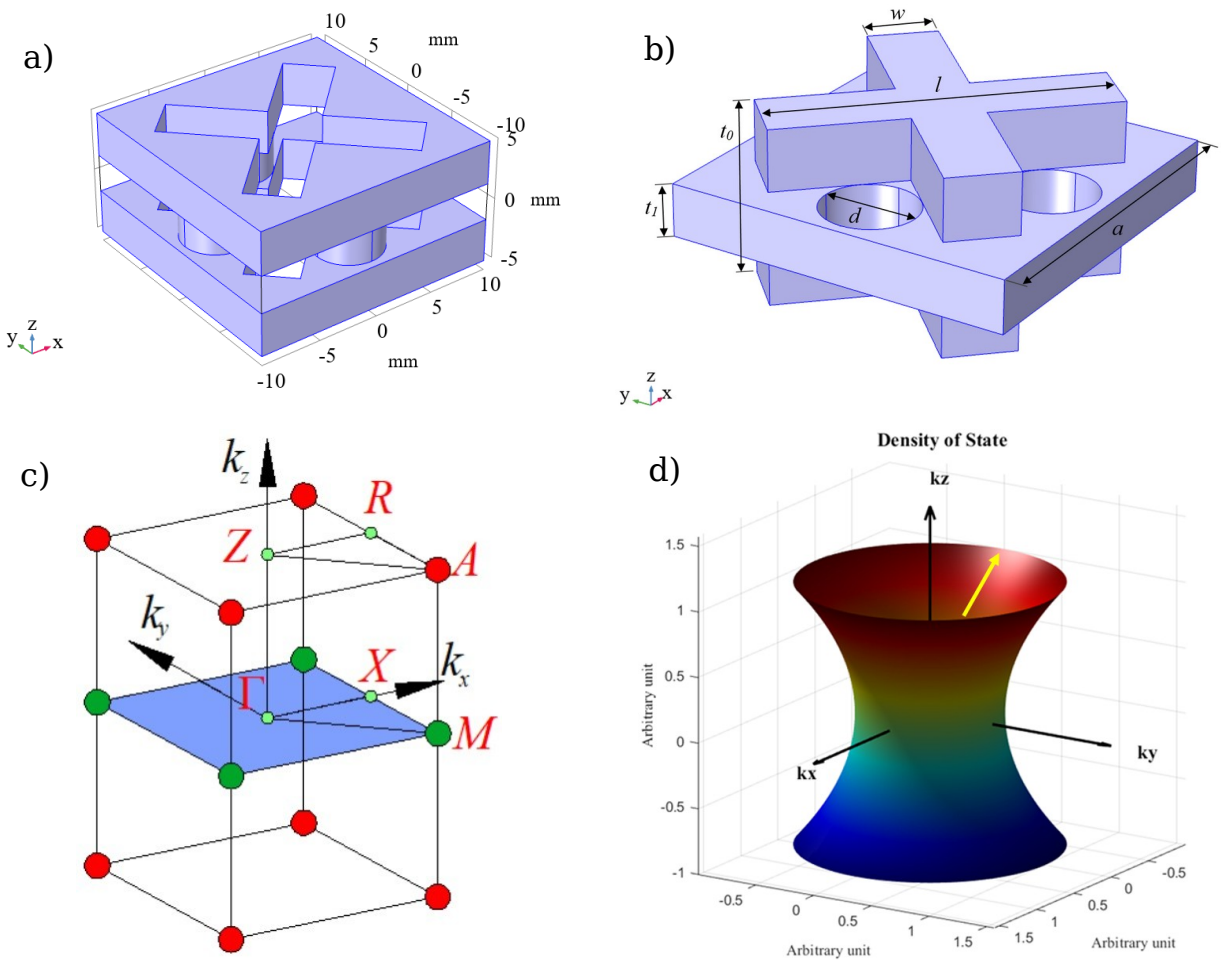

Figure 1. a) Unit cell of the phononic crystal. (3D lattice with solid inclusion for the PC, composed of vertical crossed scatterers in each layer and 4 chiral tubes connecting the 2 layers). b) Dimensions of the unit cell. The dimensions of the unit cell are a=2 cm, l=0.95a, w=0.2a, d=0.27a, t_0=0.5a, t_1=0.15a, respectively. c) First Brillouin zone with PC (green – topological charge of +1, blue – topological charge of – 1). d) Dispersion relation for an anisotropic medium. The yellow arrow denotes an allowed wavevector. The phononic density of states is related to the volume of a shell bounded between two such spheroids corresponding to two frequencies and a dispersion relation allowing unbounded values of the wavevector (yellow arrow), due to which the phononic density of states diverges.

2. Result and Discussion

We show the band structure of the unit cell along the high symmetry points and directions of the first Brillouin zone (*BZ*) at k_z=0 in Fig. 2.

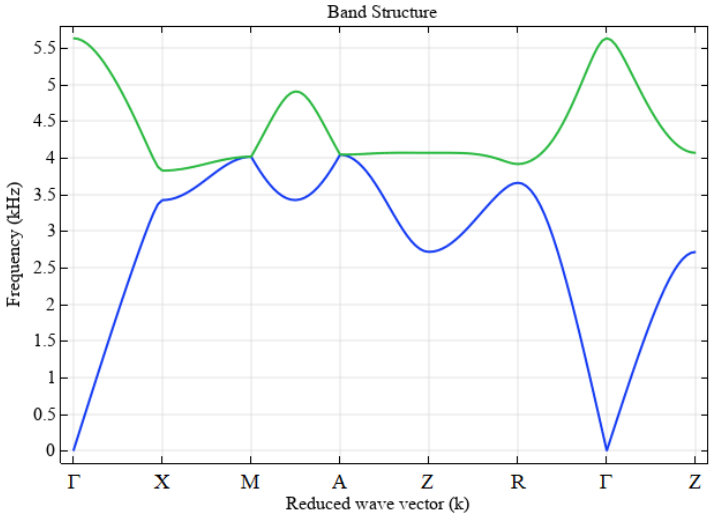

Figure 2. Band structure of the unit cell (Fig.1.c) along high symmetry points and directions of the first *BZ*.

We observe that the 1st and 2nd bands, predominantly with out-of-plane polarization, are degenerate at the *M* (around 3.92 kHz) high symmetry point. This is the first Weyl point in the system. We calculate the Weyl charge by fitting the dispersion diagram of a 2-band Hamiltonian around the Weyl point and obtaining a Weyl charge of -1 from this Weyl point. When we plot the dispersion diagram for $k_z=\pi/(a_o/2)$, the degeneracy of the bands is lifted, and there emerges a band gap between the 1st band and the 2nd band.

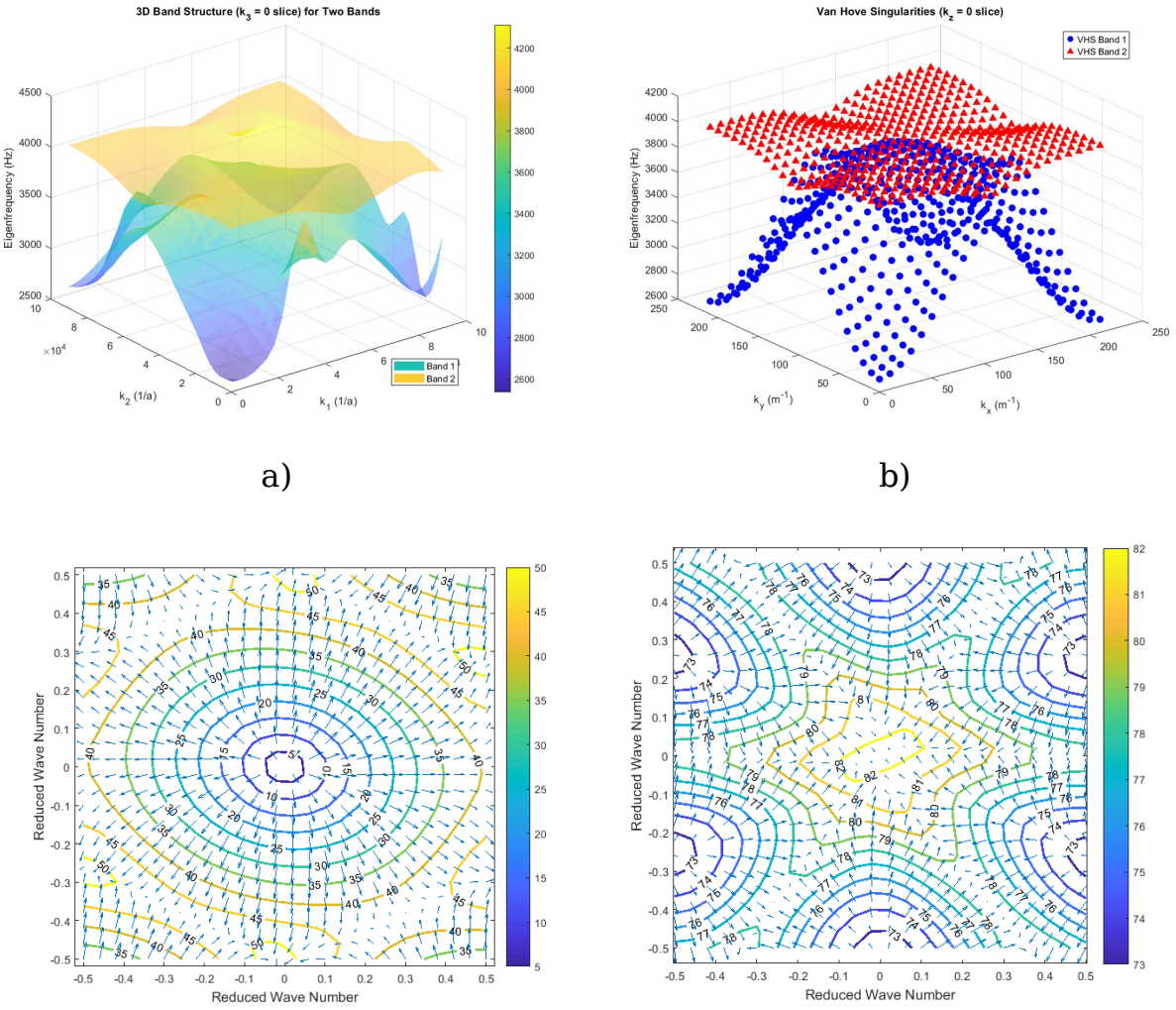

Figure 3. a) 3D band structure for two bands, b) Van Hove Singularities, c) contour plot of 1st band, and d) contour plot of 2nd band.

We increase k_z further to plot the dispersion curves at $kz=\pi/(a_o/4)$. We observe that the band gap closes again, and the two bands establish a degeneracy at 4.05 kHz and 3.75 kHz, but at the *A and R* points of the Brillouin zone instead of the *M* point, respectively. These are the second and third Weyl points in the system. As shown in the inset, we again use the two-band Hamiltonian to represent the dispersion characteristics around

this Weyl point and find that the Weyl point has +1 topological charge. In Fig. 2(d), we plot the dispersion diagram along the *X-M, M-A, and Z-R* directions to clearly visualize the Weyl degeneracy at the *A* point and the existence of a band gap between the 1st band and the 2nd band when the k_j value lies somewhere in between. The two-band Hamiltonian captures this evolution of the bands obtained through the FEA simulations reasonably well. We use this effective Hamiltonian to numerically calculate the Chern numbers of the two bands above and below the band gap for a fixed k_z. For positive k_z, these are −1 and +1 for the upper and lower bands, respectively, as marked in Fig. 2. This indicates that the band gap is topologically nontrivial.

It is easier to understand the refraction and reflection phenomena of certain waves in *k*-space since the law of conservation of momentum is met at reflection and refraction of waves. This can be best done by introducing the equifrequency surface (EFS) of the acoustic wave. This surface is obtained directly from the calculated eigenmodes inside the unit cell to form the dispersion surfaces of acoustic waves. Fig. 3a shows the dispersion surfaces of the 3D PC system for the first 2 modes.

The difference in dispersion curves in Fig. 3a is more virtually noticeable compared to Fig. 2. However, all of these dispersion surfaces hold vital information because each point on the surface gives the possible eigen solutions that consist of all the allowed wave vectors in the first Brillouin zone. It can be deduced that dispersion curves may be useful for quantitative information. Therefore, isotropic or anisotropic wave propagation of waves in PC can be best analyzed by the equal frequency contour (EFC). Figures 3c, d show the EFCs of the waves at some different frequencies in the PC crystal. The contours in Fig. 3c and d are similar in shape and circular at first for points close to the center. However, the contours become non-circular at higher frequency values. The deviation from circular shape is faster than orientation. This deviation simply implies an anisotropic phase velocity of the longitudinal acoustic wave. Fig. 3c and

d show that the contours are also non-circular, which means phase velocity depends on wave propagation direction. Moreover, all of these can be understood much better by a known approach known as the conventional approach. The conventional approach is that a straight line from the central point to another point on a contour gives the direction of the phase velocity, while the direction of velocity of energy is presented by the normal direction on the contour. Therefore, deviation from circular contour accounts for the different directions of phase and energy velocities.

3. Acoustic Metamaterials Van Hove singularity(VHS): theory and results

DOS for interband transitions as a function of energy (*E*) or frequency shows strong variations in the neighborhood of particular values of *E*, which are called critical point energies. We see that singularities in the *DOS* are expected when

$$\nabla_k E_c(k) - \nabla_k E_v(k) = 0 \qquad (1)$$

Critical points of this type occur in general at high symmetry points or at any k vector of the Brillouin zone (*BZ*). The number of critical points that may occur in the *BZ* has been discussed and analyzed by Van Hove [6]. The analytical behavior of *DOS* near the singularity may be found by expanding [$E_c(k) - E_v(k)$] in a Taylor series about the critical point. Limiting the expansion to quadratic terms and denoting the wave vectors along the principal axes with the origin at the critical point by $\boldsymbol{k}_x$, $\boldsymbol{k}_y$, $\boldsymbol{k}_z$ (eq.1),

$$E_c(k) - E_v(k) = E_0 + \left(\frac{h^2}{2}\right)\left[\varepsilon_x\left(\frac{k_x^2}{m_x}\right) + M_y\left(\frac{k_y^2}{m_y}\right) + \varepsilon_z\left(\frac{k_z^2}{m_z}\right)\right] \quad (2)$$

with m_x , m_y , and m_z positive quantities and ε_x, M_y, ε_z equal to +1 or -1 (eq.2).

We obtain four types of singularities, depending on the sign of ε_i(i= x, y, and z). The critical points are called: M_0 (all ε_i coefficients of the quadratic expansion are positive, minimum), M_1 (two ε_i coefficients of the quadratic expansion are positive and one negative, saddle point), M_2 (two ε_i coefficients of the quadratic expansion are negative and one positive, saddle point), and M_3 (all ε_i coefficients of the quadratic expansion are negative, maximum). Our results on calculating the VHS are presented in Fig. 3b. We notice that the behaviour of the DOS near critical points for the 3D case has sharp discontinuities at the critical points. The calculation presented in Fig. 3b clearly shows the presence of a VHS of a M0 type (0.1 kHz) in the Γ point of BZ, and saddle type singularity (M_1 and M_2) at the frequency region between 3.9 and 4.3 kHz, and in high symmetry points M and A of BZ, respectively.

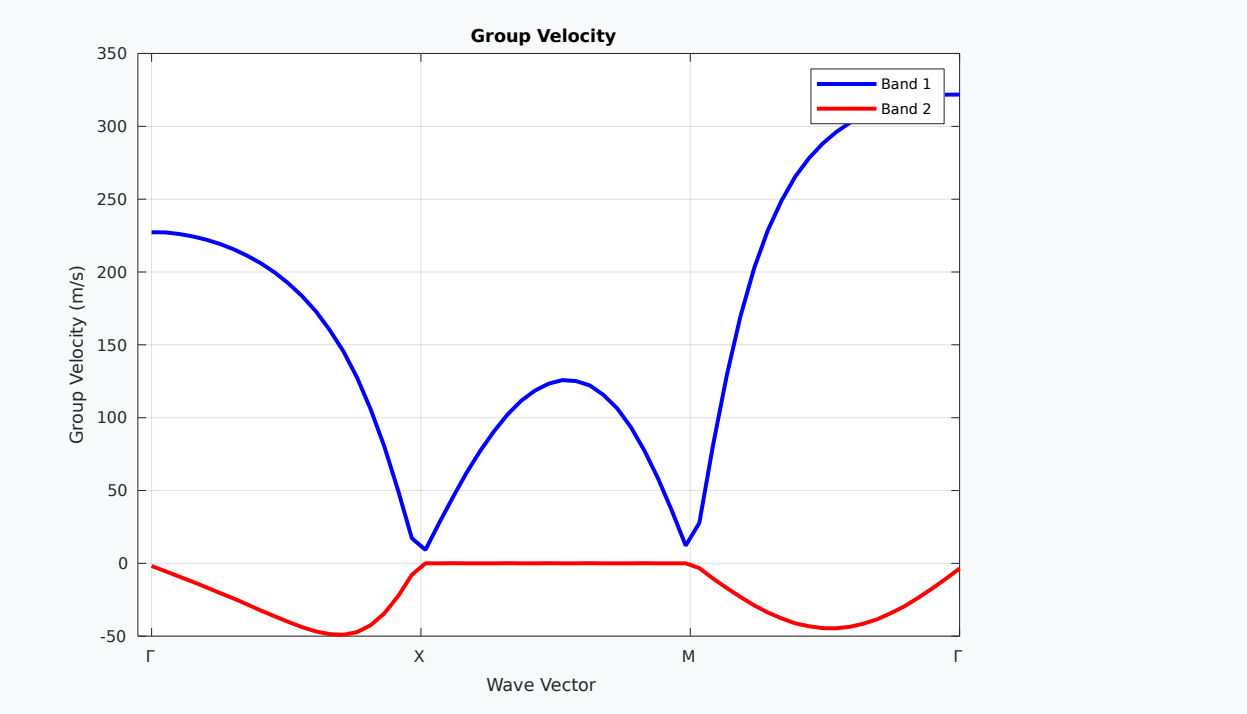

Figure 4. The first two-branch group velocity $d\omega/dk$ calculated along high symmetry directions of the first irreducible Brillouin zone.

We also calculate the group velocity for this system. It is well known that the unusually large angles (~ 180°) between the phase and group velocities of acoustic waves lead to many unusual wave phenomena observed at crystal-air or crystal-isotropic medium interfaces. In order to understand the dynamics of wave propagation, the concept of group velocity may be useful from the viewpoint of energy transportation. The direct calculation of the derivative of the dispersion relation, calculated numerically, is not always convenient and can give errors. Thus, by using the results of citation [7-9] the group velocity can always be calculated more accurately, irrespective of the number of points in the dispersion curve. Therefore, we have calculated the group velocity along the high-symmetry directions Γ-X-M-Γ of the BZ as shown in Fig. 4. From Fig. 4, it is evident that the components of the group velocity versus the high symmetry direction (Γ-X-M) vary over wide limits. The dependences v_g, which describe the wave packets of localized modes of any order, exhibit (generally) a maximum at

certain propagation constants. This means that the dispersion of group velocity can be positive, negative or zero citation [8, 9]. It is worth mentioning that the group velocity of the waves is zero at the high symmetry direction between *X*-*M*, meaning that there is no energy transfer in this direction.

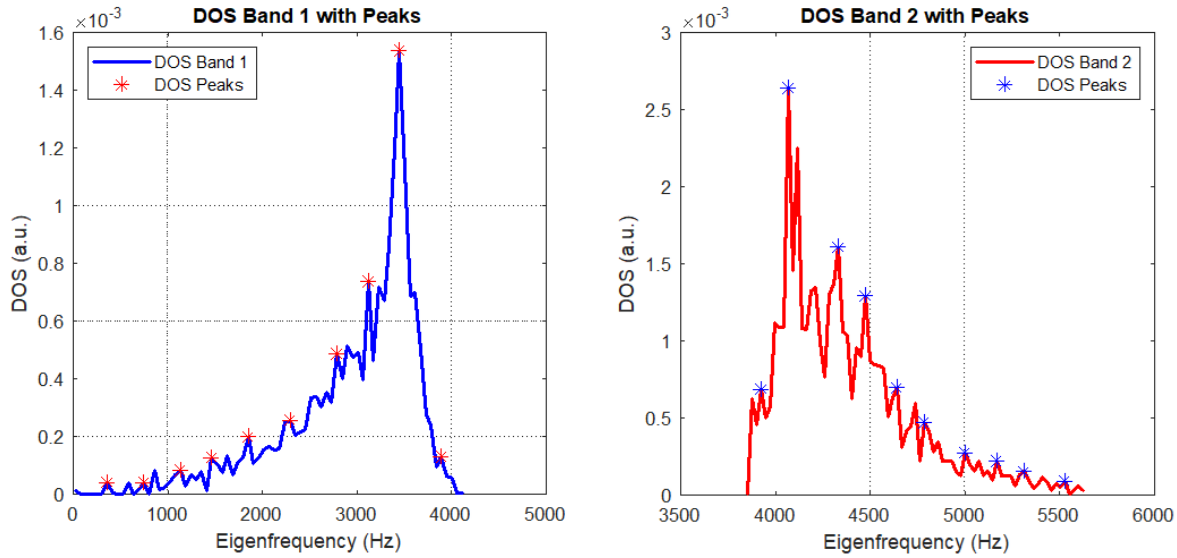

Figure 5. DOS with peaks for a) band 1, b) for band 2

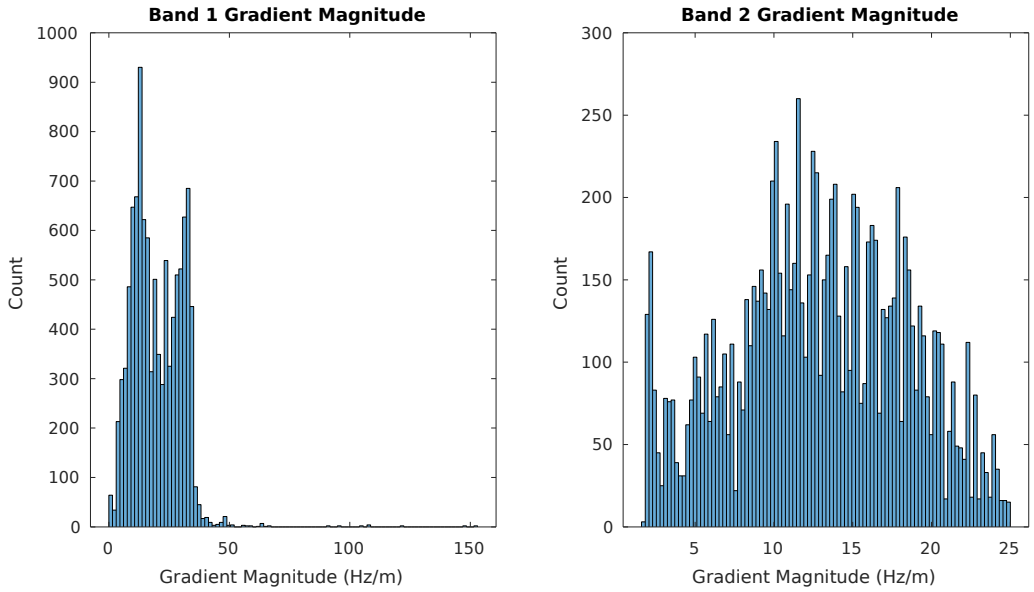

Figure 6. Gradient magnitude a) for band 1, b) for band 2

The band structure of a crystal system with two energy bands was analysed to identify Van Hove singularity (VHS) points, calculate the density of states (DOS), and determine the corresponding peaks (Fig. 5). The input dataset consisted of normalised k-points (k_1, k_2, k_3) and the associated eigenfrequencies of the two bands, which were imported from a spreadsheet file. These k-points were converted into physical wavevector components (k_x, k_y, k_z) for evaluation in reciprocal space. The gradients of the eigenfrequencies were computed for each band (eq. 3), their magnitudes were determined (eq. 4), and the resulting intervals were examined. From these calculations, the DOS and VHS peaks were obtained and subsequently presented in graphical and tabular form (Fig. 6).

$$\nabla E = \left(\frac{\partial E}{\partial k_x}, \frac{\partial E}{\partial k_y}, \frac{\partial E}{\partial k_z} \right) \quad (3)$$

$$|\nabla E| = \sqrt{\left(\left(\frac{\partial E}{\partial k_x} \right)^2 + \left(\frac{\partial E}{\partial k_y} \right)^2 + \left(\frac{\partial E}{\partial k_z} \right)^2 \right)} \quad (4)$$

The gradient of the band structure in reciprocal space (k-space) was evaluated to determine the rate of change of the eigenfrequencies, expressed in Hz/m. Van Hove singularities (VHS) were identified as points where the gradient magnitude $|\nabla E|$ falls below a threshold value of 10, corresponding to nearly flat regions of the dispersion. The analysis was restricted to the k_z=0 slice of the Brillouin zone, where VHS points were located and their corresponding energy values recorded. These VHSs represent critical points of the band structure—minima, maxima, or saddle points—where the gradient approaches zero, giving rise to singular features in the density of states (DOS).

To compute the DOS, the energy values were flattened and processed using a histogram-based approach according to the relation in eq. 5:

$$DOS(E) \propto \int \delta(E - E(k))\, dk \quad (5)$$

The resulting DOS values were reported together with the corresponding energy intervals. Peaks in the DOS were extracted and identified as indicators of VHS, since they signify regions of high state density. The peak energies were calculated in multiple units Hz, eV, and Joules using the relations in eq. 6:

$$E_{eV} = E_{Hz} . h_{eV}, E_J = E_{Hz} . h_J \quad (6)$$

with h_{eV}=4.135667696×10^{-15} eV\cdotps and h_J=6.62607015×10^{-34} J\cdotps. The correspondence between VHS points and DOS peaks provides a direct link between band structure topology and state density.

Conclusion

In summary, we have designed a 3D mechanical structure analogous to the honeycomb lattice. We show that this relatively simple design carries Weyl

points at the vertices of the Brillouin zone and describe the dynamics around the Weyl points and calculate their topological charges. We show the finite boundaries of this structure. Using numerical simulations on a 3D structure, we show the existence of Fermi arcs and compare them with the results obtained from equifrequency-contour analysis. Our design could be easily scaled up or down and can be relevant to applications such as energy harvesting and vibration control on 3D elastic structures.

Acknowledgment

The author (Ekmel Ozbay) acknowledges partial support from the Turkish Academy of Sciences.

References

[1.] Li F, Huang X, Lu J, Ma J and Liu Z: Weyl points and Fermi arcs in a chiral phononic crystal. Nature Phys. 2017; 14: 30-35.

[2.] Xu SY et al: Discovery of a Weyl fermion semimetal and topological Fermi arcs. Science. 2015; 349: 613–617.

[3.] Lu L, Fu L, Joannopoulos J D & Soljacic M: Weyl points and line nodes in gyroid photonic crystals. Nat. Photon. 2013; 7: 294–299.

[4.] Yang Z, Zhang B: Acoustic type-II Weyl nodes from stacking dimerized chains. Phys. Rev. Lett. 2016; 117: 224301.

[5.] Soluyanov AA. et al.: Type-II Weyl semimetals. Nature. 2015; 527: 495–498.

[6.] Bassani F., Pastori Parravicini G.: Electronic States and Optical Properties in Solids, Oxford: Pergamon Press (1975).

[7.] A. Srivastava, Elastic metamaterials and dynamic homogenization: a review. Int. J. of Smart and Nano Materials 6(1), 41–60 (2015).

[8.] V. A. Burov, V. B. Voloshinov, K. V. Dmitriev, N. V. Polikarpova, Acoustic waves in metamaterials, crystals, and anomalously refracting structures. Phys. Usp. 181(11), 1205–1211 (2011).

[9.] 16. R. V. Craster, S. Guenneau, Acoustic Metamaterials: Negative Refraction, Imaging, Lensing and Cloaking. New York: Springer Series in Materials Science (2013)